

Observation of a Novel Orbital Selective Mott Transition in $\text{Ca}_{1.8}\text{Sr}_{0.2}\text{RuO}_4$

M. Neupane,¹ P. Richard,^{1,2} Z.-H. Pan,¹ Y.-M. Xu,¹ R. Jin,³ D. Mandrus,³ X. Dai,⁴ Z. Fang,⁴ Z. Wang,¹ and H. Ding^{1,4}

¹*Department of Physics, Boston College, Chestnut Hill, Massachusetts 02467, USA*

²*WPI-AIMR, Tohoku University, Sendai 980-8578, Japan*

³*Condensed Matter Science Division, Oak Ridge National Laboratory, Oak Ridge, Tennessee 37831, USA*

⁴*Beijing National Laboratory for Condensed Matter Physics, and Institute of Physics, Chinese Academy of Sciences, Beijing 100190, China*

(Received 11 December 2008; published 25 August 2009)

We observed a novel orbital selective Mott transition in $\text{Ca}_{1.8}\text{Sr}_{0.2}\text{RuO}_4$ by angle-resolved photoemission. While two sets of dispersing bands and the Fermi surface associated with the doubly degenerate d_{yz} and d_{zx} orbitals are identified, the Fermi surface associated with the wider d_{xy} band is missing as a consequence of selective Mott localization. Our theoretical calculations demonstrate that this orbital selective Mott transition is mainly driven by the combined effects of interorbital carrier transfer, superlattice potential, and orbital degeneracy, whereas the bandwidth difference plays a less important role.

DOI: 10.1103/PhysRevLett.103.097001

PACS numbers: 74.70.Pq, 71.30.+h, 79.60.-i

$\text{Ca}_{2-x}\text{Sr}_x\text{RuO}_4$ is a fascinating $4d$ multiorbital system that exhibits a rich and intricate phase diagram, ranging from a chiral p -wave superconductor (Sr_2RuO_4) to a Mott insulator (Ca_2RuO_4) [1,2]. Similar to the high- T_c cuprates, the metal-insulator transition under the influence of electron correlations in the ruthenates is of fundamental importance and currently under intensive debate. There is accumulating experimental evidence for the coexistence of local moments and metallic transport, and heavy fermion behavior in the region of $0.2 \leq x \leq 0.5$ [2–4], which is remarkable because there are no f electrons in this material. To account for the coexistence of localized and itinerant electrons in this region, the scenario of orbital selective Mott transition (OSMT) has been proposed [5,6] as following: Sr_2RuO_4 has three degenerated t_{2g} orbitals (d_{xy} , d_{yz} , and d_{zx}) occupied by four $4d$ electrons. The isovalent Ca substitute does not change the total carrier concentration, but rather increases the effective electron correlation strength (U_{eff}) relative to the reduced bandwidth which is induced by structural change due to the smaller ion radius of Ca^{2+} . Consequently, it is possible that an OSMT takes place in the narrower bands, i.e., the one-dimensional (1D) d_{yz} and d_{zx} orbitals, where electrons undergo a Mott transition and become localized, while the electrons in the wider two-dimensional (2D) d_{xy} band remain itinerant. A similar partial localization mechanism has been proposed for some heavy fermion materials, e.g., UPd_2Al_3 [7].

While the concept of OSMT is of critical importance to the multiorbital Mott Hubbard systems and has been studied extensively in theory [5,6,8–10], it has not been confirmed experimentally. Our previous angle-resolved photoemission spectroscopy (ARPES) study [11] shows that, for samples with $x = 0.5$, the two 1D (α and β) Fermi surface (FS) sheets are clearly “visible” as well as that of the 2D (γ) FS, although the latter is considerably smeared and weaker in comparison to the case of Sr_2RuO_4 . This is in sharp contrast to the OSMT prediction that the

1D FS sheets become Mott localized. To check if the OSMT occurs at a lower Sr concentration, we have conducted ARPES experiments on high-quality single crystals at $x = 0.2$, grown by the floating zone technique [4].

Our experiments were performed at synchrotron undulator beam lines (e.g., Wadsworth, U1-NIM, PGM at the Synchrotron Radiation Center, Wisconsin), using a Scienta SES-2002 electron analyzer. The energy and momentum resolutions are 10–30 meV and 0.02 \AA^{-1} , respectively. Samples were cleaved *in situ* and measured at 40 K in a vacuum better than 1×10^{-10} torr. The samples have been found to be stable and without degradation for a typical measurement period of 48 hours. Precise determination of the low-energy electronic structure at this doping level is a rather difficult and lengthy experiment due to a much reduced ARPES spectral intensity in the vicinity of the Fermi energy (E_F) near the insulating phase. Several techniques have been used to boost photoelectron signals, including enhancement of the ARPES matrix elements through fine-tuning of photon energy and measurements at different Brillouin zones (BZs). Laue pictures have been taken before the measurement to align the samples, and LEED pictures of the surface have also been recorded. These pictures, which are included in the supplementary material [12], clearly indicate good quality of samples and cleaved surfaces.

As shown in Fig. 1, strong spectral intensity and clear dispersion similar to the case of Sr_2RuO_4 are observed in the valence band of $\text{Ca}_{1.8}\text{Sr}_{0.2}\text{RuO}_4$. However, the spectral intensity near E_F experiences dramatic reductions as the Sr content x approaches 0.2, as demonstrated in Fig. 1(c), reflecting the fact that the system is near an insulating phase. To see clearly the low-energy excitations, we zoom in to the binding energy range within 0.2 eV to E_F , as plotted in Fig. 2. One can identify weak but discernible peaks dispersing towards E_F , as shown in Figs. 2(c) and 2(d). Unlike Sr_2RuO_4 , which has Fermi

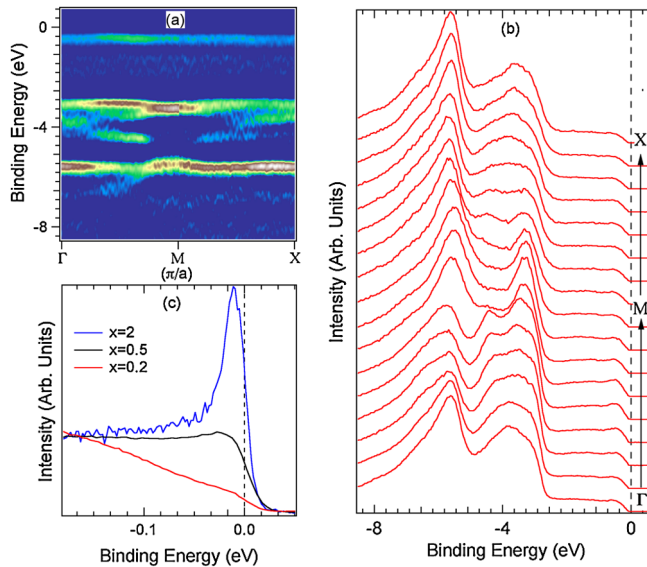


FIG. 1 (color online). The valence band of $\text{Ca}_{1.8}\text{Sr}_{0.2}\text{RuO}_4$. (a) Plot of second derivative of ARPES intensity for the valence band of $\text{Ca}_{1.8}\text{Sr}_{0.2}\text{RuO}_4$ taken along Γ - M - X ($h\nu = 75$ eV, $T = 40$ K). (b) The corresponding EDCs along Γ - M - X . (c) Comparison of the EDCs for $x = 0.2, 0.5, 2$, taken at the β band crossing point along Γ - M ($h\nu = 32$ eV, $T = 40$ K).

liquidlike quasiparticle (QP) peaks [13], $\text{Ca}_{1.8}\text{Sr}_{0.2}\text{RuO}_4$ has a much broader line shape in its low-energy dispersion. As illustrated in Figs. 2(a) and 2(b), we observe two linearly dispersive bands along the high-symmetry line X - Γ - X , crossing E_F around 0.3 and -0.9 \AA^{-1} , respectively. These two Fermi crossing (k_F) points, plotted in

Fig. 2(f) as points 1 and 2, locate, respectively, on the calculated α FS for Sr_2RuO_4 and its folded FS (labeled as the α' FS) due to the $\sqrt{2} \times \sqrt{2}$ reconstruction caused by a rotation of the RuO_6 octahedra [14]. We note that the peak intensity in both energy distribution curves (EDCs) and momentum distribution curves (MDCs) diminishes as it approaches E_F or k_F , possibly due to a small energy gap or the QP decoherence effect observed in some transition metal oxides near the metal-insulator boundary [15]. The band dispersion along another high-symmetry line M - Γ - M is displayed in Fig. 2(e), and we observed four FS crossings (points 3–6) whose locations are plotted in Fig. 2(f). While the crossing points 4 and 5 are on the calculated α' FS, and 3 and 6 are close to the β FS with respect to the location and direction of dispersion as compared with $x = 0$ and 0.5 , there is no observation of the dispersing γ band and the corresponding FS crossing. A direct comparison of ARPES spectra between $\text{Ca}_{1.8}\text{Sr}_{0.2}\text{RuO}_4$ and Sr_2RuO_4 is included in the supplementary material [12], clearly showing the absence of the γ band for the former case.

To verify these band and FS assignments, we have performed many measurements to cover a wide range of k space. We locate and plot all observed FS crossing points in the first BZ shown in Fig. 3(a). The extracted k_F points from the dispersive bands indicated by dots are obtained from MDCs and EDCs. The uncertainty of k_F determination is estimated to be about $\pm 0.03 \text{ \AA}^{-1}$ which is $\sim 2\%$ of the BZ size ($2\pi/a$) of $\text{Ca}_{1.8}\text{Sr}_{0.2}\text{RuO}_4$. It is clear that both the α and β main FS sheets and the folded α' FS are present in $\text{Ca}_{1.8}\text{Sr}_{0.2}\text{RuO}_4$. However, no evidence of the γ FS is found. The disappearance of the γ FS is puzzling.

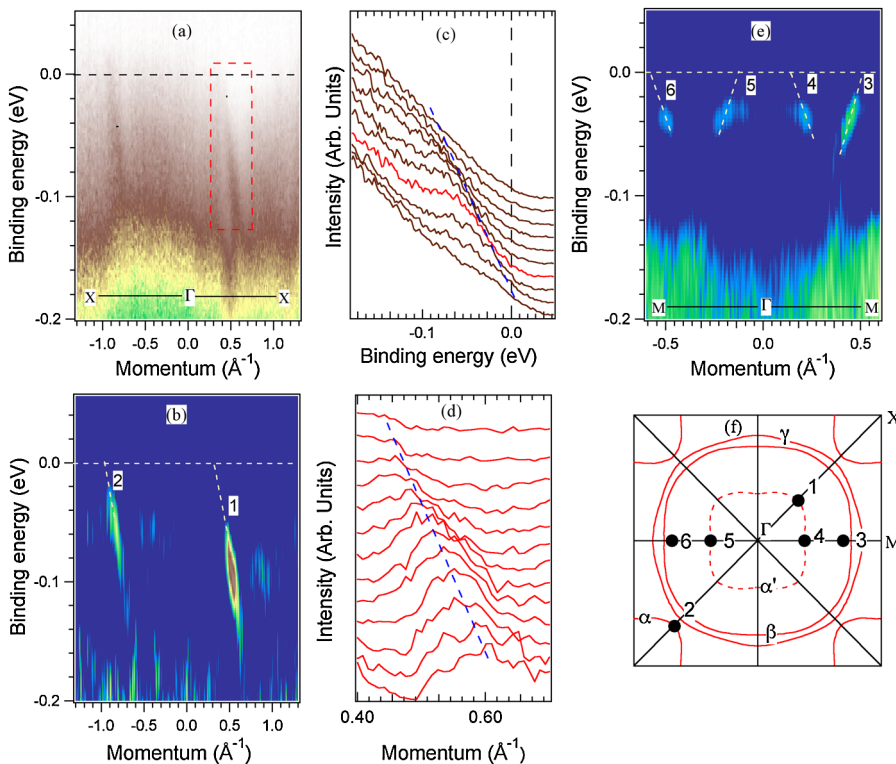


FIG. 2 (color online). Band dispersion along high-symmetry directions in $\text{Ca}_{1.8}\text{Sr}_{0.2}\text{RuO}_4$. (a) ARPES intensity plot along X - Γ - X . (b) The corresponding second derivative plot of (a). The white dashed lines are guides for eyes. (c) EDCs and (d) MDCs, within the red dashed box in (a), showing low-energy band dispersion, as indicated by blue dashed lines. (e) Second derivative plot of ARPES intensity along M - Γ - M . (f) Fermi crossings (black dots) indicated in (b) and (e), and Fermi surface sheets (red lines) calculated by LDA for Sr_2RuO_4 [21] in the first BZ.

According to the Luttinger theorem, the total occupied FS area should remain the same due to the isovalence nature of the Ca-Sr substitution. From the fitted α and β FS sheets shown in Fig. 3(a), we derive the electron occupations $n_\alpha = 1.72 \pm 0.12$ and $n_\beta = 0.79 \pm 0.06$, implying that the γ band has 1.49 ± 0.10 valence electrons since $n_{\text{total}} = 4$. To illustrate this point, we plot the “would be” γ FS in Fig. 3(a) as a simple circle (black dashed line), which satisfies the Luttinger counting of 1.49 electrons. Note that it would almost touch the M point, indicating that its van Hove singularity is very close to E_F , which may lead to instability at low temperature.

To further understand the fate of the γ band, we plot in Fig. 3(b) an EDC of $\text{Ca}_{1.8}\text{Sr}_{0.2}\text{RuO}_4$ integrated over the neighboring region of M . In contrast to Sr_2RuO_4 , $\text{Ca}_{1.8}\text{Sr}_{0.2}\text{RuO}_4$ shows a dramatic suppression of the γ QPs. In fact, the spectrum consists of a broad feature with a gap of ≥ 100 meV, and a small “foot” extending toward E_F . The origin of this small foot is not entirely

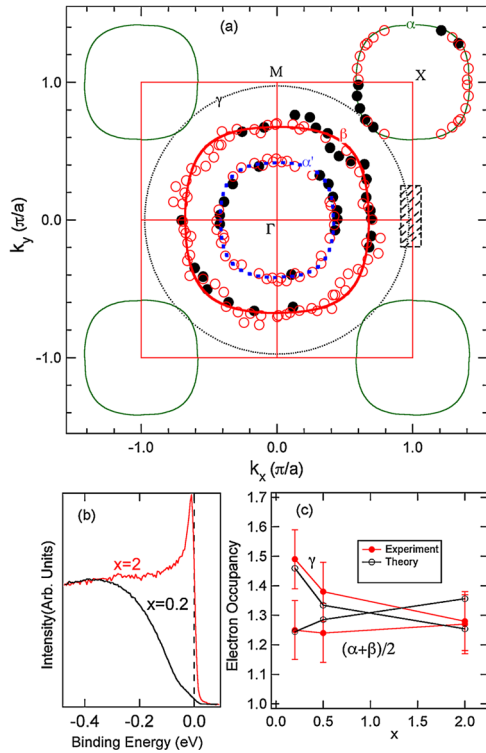


FIG. 3 (color online). Fermi surface and electron occupancy of different orbitals. (a) Measured FS sheets of α (green contours centered at X), β (red contour centered at Γ), and the folded α (blue dashed contour centered at Γ), along with the Fermi crossing points determined by ARPES (black solid dots) and symmetrized points according to the fourfold crystal symmetry (red open dots). The black dotted contour centered at Γ is the derived γ FS according to the Luttinger theorem. (b) Comparison of the EDCs at M between $\text{Ca}_{1.8}\text{Sr}_{0.2}\text{RuO}_4$ and Sr_2RuO_4 , integrated over the k region indicated by the shaded rectangle in (a). (c) The Sr content dependence of electron occupancy of γ and $(\alpha + \beta)/2$, obtained by ARPES (red filled dots and lines), and LDA (black open dots and lines).

clear, although it may come from a residual γ band from a minority phase, or certain impurity states. We regard the disappearance of the γ QP with a large soft gap as evidence for localization of the γ band. We notice that the electron occupancy of the γ band is close to 1.5 (a half integer) from both the experimental derivation and our theoretical calculation using local density approximation (LDA), as shown in Fig. 3(c). It is remarkable that the LDA calculation shows good agreement with the ARPES observation. The basic reason for the increase of the γ electron occupation is that the increased hybridization between the t_{2g} and e_g orbitals, due to the increasing rotation and tilting of the octahedra at higher Ca content, pushes down the d_{xy} band [10]. The same effect has been also observed in a similar $4d$ -electron system (Sr_2RhO_4) [16].

A natural question is why the γ FS is absent at 1.5 electron occupancy. Remarkably, as the system undergoes the $\sqrt{2} \times \sqrt{2}$ reconstruction in the bulk [14], the γ band folds into two subbands by the superlattice potential, accompanied by the doubling of the unit cell. The folded γ bands in the reduced BZ host a total of 3 electrons. The lower subband is completely filled, while the upper one is precisely at half-filling. It is thus possible for the γ complex to undergo the Mott transition and become localized in the doubled unit cell, contributing a spin-1/2 local moment. Since there are two Ru atoms per supercell, the localized magnetic moment is $0.5\mu_B$ per Ru atom. This is indeed consistent with the field dependent magnetization measurement in $\text{Ca}_{1.8}\text{Sr}_{0.2}\text{RuO}_4$ [3]. The sharp increase of the magnetization to $0.5\mu_B$ as the applied magnetic field reaches about 5 T can be attributed naturally to the polarization of the local moment, whereas the subsequent gradual growth of the magnetization with further increasing field arises from Pauli paramagnetism of the itinerant α and β band electrons.

Theoretically, most of the model studies have focused on the two-band Hubbard model, where the OSMT is mainly controlled by the difference in the bandwidths [6,8]. The real situation in the $\text{Ca}_{2-x}\text{Sr}_x\text{RuO}_4$ system is more complex. Because of the $\sqrt{2} \times \sqrt{2}$ superstructure, there is a total of six bands occupied by eight electrons in the doubled unit cell. We have carried out first-principle calculations and found that the lower three bonding bands are fully occupied by six electrons. The remaining two electrons occupy the upper three antibonding bands. If there were no crystal field splitting, these two electrons would be almost evenly distributed among the upper three bands, corresponding to occupations (2/3, 2/3, 2/3). However, the localized orbital must be filled by an odd integer number of electrons in an OSMT, which can be realized in $\text{Ca}_{2-x}\text{Sr}_x\text{RuO}_4$ only when the two electrons redistribute among the upper three bands to reach occupations (1/2, 1/2, 1) due to the crystal field splitting. Indeed, our LDA calculation shows that, with the reduction of x , the crystal field pulls down the γ band and transfers charge from the α , β bands to the γ band as shown in Fig. 3(c). When the

electron distribution reaches $(1/2, 1/2, 1)$, the three-band complex splits into two groups: two nearly degenerate α and β bands, and a separated γ band with a lowered center of gravity. Therefore, we have one two-band system and one single-band system, both with one electron per unit cell. The reason for the OSMT to take place in the γ band is that the critical interaction U_c for the Mott transition in a single-band Hubbard model is about 30% smaller than that of a two-band model with one electron per unit cell and identical bandwidth, a result obtained by variational Gutzwiller and dynamical mean field theory [17,18]. The Hund's rule coupling further increases the critical U_c for the two-band system. Therefore, in a large area of the parameter space, the single γ -band system lies in the Mott phase, while the two-band system remains in the metallic phase. The new type of OSMT induced by the orbital degeneracy lifting has been studied theoretically in detail in Ref. [19].

To further illustrate this point, we apply the slave boson mean field theory to a simple three-band Hubbard model with the bandwidth ratios of 1:1:1 and 1:1:1.5 and two electrons per unit cell. The technical details have been explained in Ref. [20]. In Fig. 4, we plot the QP coherence weight (Z) and the orbital correlations as a function of the charge transfer δ . Figure 4(a) clearly shows that the coherence weight of the γ band decreases continuously while that of the degenerate α band remains almost a constant as the OSMT is approached at charge transfer $\delta = 1/3$,

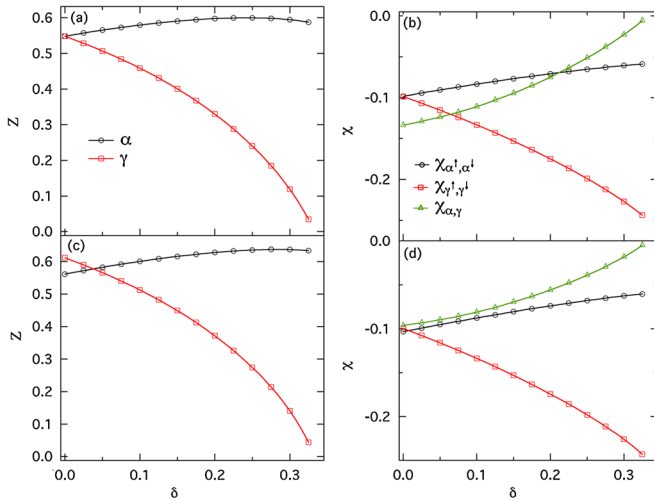


FIG. 4 (color online). Calculations that show OSMT in multi-orbital systems. (a) QP weight for the 3-band Hubbard model with equal bandwidth W as a function of charge transfer δ defined by $(n_\alpha, n_\beta, n_\gamma) = (\frac{2}{3} - \frac{\delta}{2}, \frac{2}{3} - \frac{\delta}{2}, \frac{2}{3} + \delta)$. $U/W = 4.0$; $J/W = 1.0$. (b) Intra and interband correlation functions, where $\chi_{\alpha^1, \alpha^1} = \langle n_{\alpha^1} n_{\alpha^1} \rangle - \langle n_{\alpha^1} \rangle \langle n_{\alpha^1} \rangle$, $\chi_{\gamma^1, \gamma^1} = \langle n_{\gamma^1} n_{\gamma^1} \rangle - \langle n_{\gamma^1} \rangle \langle n_{\gamma^1} \rangle$, and $\chi_{\alpha, \gamma} = \langle (n_{\alpha^1} + n_{\alpha^2})(n_{\gamma^1} + n_{\gamma^2}) \rangle - \langle (n_{\alpha^1} + n_{\alpha^2}) \rangle \langle (n_{\gamma^1} + n_{\gamma^2}) \rangle$. (c) Same as in (a), except for the three bandwidths of W , W , $1.5W$. (d) Same as in (b), except for the three bandwidths of W , W , $1.5W$. Note that the y axis is negative in (b) and (d). With increasing δ , the intra- γ -band correlation becomes large and negative, while the interband correlation approaches zero.

which corresponds to the charge distribution $(1/2, 1/2, 1)$. Concomitantly, as can be seen from Fig. 4(b), the interband correlations (χ) between the γ and the α , β bands are dramatically reduced. To verify that the bandwidth difference does not play an important role in the OSMT, we show in Figs. 4(c) and 4(d) that the same conclusion is reached for the case where the γ band is 1.5 times as wide as that of the α and β bands.

In conclusion, we have measured the low-energy excitations in $\text{Ca}_{2-x}\text{Sr}_x\text{RuO}_4$ near $x = 0.2$ by ARPES and unraveled a novel mechanism for the OSMT. The band dispersions and the associated FSs are observed for the d_{yz} and d_{zx} orbitals. In contrast, the d_{xy} orbital shows a loss of coherent QP excitations due to Mott localization. We discovered that the $\sqrt{2} \times \sqrt{2}$ structure reconstruction plays a crucial role in establishing the half-filling condition of the antibonding γ band. We provided microscopic theoretical support for this novel OSMT and demonstrated the importance of the crystal-field-splitting-induced interorbital charge transfer and the orbital degeneracy for promoting an intriguing electronic phase with coexisting local moment and itinerant electrons.

This work was supported by grants from the U.S. NSF DMR-0704545, DOE DEFG02-99ER45747, and China NSF. This work is based upon research conducted at the Synchrotron Radiation Center supported by the NSF DMR-0537588. Oak Ridge National laboratory is managed by UT-Battelle, LLC, for the DOE under Contract No. DE-AC05-00OR22725.

- [1] Y. Maeno *et al.*, Nature (London) **372**, 532 (1994).
- [2] S. Nakatsuji and Y. Maeno, Phys. Rev. Lett. **84**, 2666 (2000).
- [3] S. Nakatsuji *et al.*, Phys. Rev. Lett. **90**, 137202 (2003).
- [4] R. Jin *et al.*, arXiv:0112405.
- [5] V.I. Anisimov *et al.*, Eur. Phys. J. B **25**, 191 (2002).
- [6] A. Koga *et al.*, Phys. Rev. Lett. **92**, 216402 (2004).
- [7] N. Sato *et al.*, Nature (London) **410**, 340 (2001).
- [8] A. Liebsch, Phys. Rev. Lett. **91**, 226401 (2003).
- [9] A. Liebsch and H. Ishida, Phys. Rev. Lett. **98**, 216403 (2007).
- [10] Z. Fang, N. Nagaosa, and K. Terakura, Phys. Rev. B **69**, 045116 (2004).
- [11] S.-C. Wang *et al.*, Phys. Rev. Lett. **93**, 177007 (2004).
- [12] See EPAPS Document No. E-PRLTAO-103-055936 for supplementary material containing more experimental details. For more information on EPAPS, see <http://www.aip.org/pubservs/epaps.html>.
- [13] N.J.C. Ingle *et al.*, Phys. Rev. B **72**, 205114 (2005).
- [14] R. Matzdorf *et al.*, Science **289**, 746 (2000).
- [15] D.S. Dessau *et al.*, Phys. Rev. Lett. **81**, 192 (1998).
- [16] B.J. Kim *et al.*, Phys. Rev. Lett. **97**, 106401 (2006).
- [17] S. Florens *et al.*, Phys. Rev. B **66**, 205102 (2002).
- [18] J.P. Lu, Phys. Rev. B **49**, 5687 (1994).
- [19] L. de'Medici *et al.*, Phys. Rev. Lett. **102**, 126401 (2009).
- [20] X. Dai, G. Kotliar, and Z. Fang, arXiv:0611075.
- [21] T. Oguchi *et al.*, Phys. Rev. B **51**, 1385 (1995).